



Lineage-specific differentiation of osteogenic progenitors from pluripotent stem cells reveals the FGF1-RUNX2 association in neural crest-derived osteoprogenitors

Fahad Kidwai¹  | Byron W. H. Mui¹ | Deepika Arora^{1,2} | Kulsum Iqbal³ |
Madison Hockaday¹ | Luis Fernandez de Castro Diaz⁴ | Natasha Cherman¹ |
Daniel Martin⁵ | Vamsee D. Myneni⁶ | Moaz Ahmad⁷ | Katarzyna Futrega¹ |
Sania Ali⁸ | Randall K. Merling¹ | Dan S. Kaufman⁹  | Janice Lee¹⁰ |
Pamela G. Robey¹

¹Department of Health and Human Services, Craniofacial and Skeletal Diseases Branch, National Institute of Dental and Craniofacial Research, National Institutes of Health, Bethesda, Maryland

²Biosystems and Biomaterials Division, National Institute of Standards and Technology, Gaithersburg, Maryland

³Department of Health and Human Services, Dental Consult Services, National Institute of Health Dental Clinic, Bethesda, Maryland

⁴Department of Health and Human Services, Skeletal Disorders and Mineral Homeostasis Section, National Institute of Dental and Craniofacial Research, National Institutes of Health, Bethesda, Maryland

⁵Department of Health and Human Services, Genomics and Computational Biology Core, National Institute of Dental and Craniofacial Research, National Institutes of Health, Bethesda, Maryland

⁶Department of Health and Human Services, Craniofacial and Skeletal Diseases Branch/Adult Stem Cell Section, National Institute of Dental and Craniofacial Research, National Institutes of Health, Bethesda, Maryland

⁷Department of Health and Human Services, Molecular Physiology and Therapeutics Branch, National Institute of Dental and Craniofacial Research, National Institutes of Health, Bethesda, Maryland

⁸Biology of Global Health, Department of Biology, Georgetown University, Washington, District of Columbia

⁹Department of Medicine, University of California, La Jolla, California

¹⁰Department of Health and Human Services, Craniofacial Anomalies and Regeneration Section, National Institute of Dental and Craniofacial Research, National Institutes of Health, Bethesda, Maryland

Correspondence

Fahad Kidwai, DDS, MSc, PhD, and Pamela G. Robey, PhD, Department of Health and Human Services, Craniofacial and Skeletal Diseases Branch, National Institute of Dental and Craniofacial Research, National Institutes of Health, Bethesda, MD 20892.
Email: fahad.kidwai@nih.gov (F. K.) and
Email: probey@dir.nidcr.nih.gov (P. G. R.)

Funding information

Colgate-Palmolive Company; American Association for Dental Research; Genentech; Doris Duke Charitable Foundation; National Institute of Health, Grant/Award Numbers: DE022556, DE000727, DE000380

Abstract

Human pluripotent stem cells (hPSCs) can provide a platform to model bone organogenesis and disease. To reflect the developmental process of the human skeleton, hPSC differentiation methods should include osteogenic progenitors (OPs) arising from three distinct embryonic lineages: the paraxial mesoderm, lateral plate mesoderm, and neural crest. Although OP differentiation protocols have been developed, the lineage from which they are derived, as well as characterization of their genetic and molecular differences, has not been well reported. Therefore, to generate lineage-specific OPs from human embryonic stem cells and human induced pluripotent stem cells, we employed stepwise differentiation of paraxial mesoderm-like cells,

Fahad Kidwai, Byron W. H. Mui and Deepika Arora contributed equally as the first author.

This is an open access article under the terms of the Creative Commons Attribution-NonCommercial License, which permits use, distribution and reproduction in any medium, provided the original work is properly cited and is not used for commercial purposes.

©2020 The Authors. STEM CELLS published by Wiley Periodicals LLC on behalf of AlphaMed Press 2020

lateral plate mesoderm-like cells, and neural crest-like cells toward their respective OP subpopulation. Successful differentiation, confirmed through gene expression and *in vivo* assays, permitted the identification of transcriptomic signatures of all three cell populations. We also report, for the first time, high FGF1 levels in neural crest-derived OPs—a notable finding given the critical role of fibroblast growth factors (FGFs) in osteogenesis and mineral homeostasis. Our results indicate that FGF1 influences RUNX2 levels, with concomitant changes in ERK1/2 signaling. Overall, our study further validates hPSCs' power to model bone development and disease and reveals new, potentially important pathways influencing these processes.

KEYWORDS

bone development, cell differentiation, fibroblast growth factor 1, neural crest, osteogenesis, pluripotent stem cells

1 | INTRODUCTION

Human pluripotent stem cells (hPSCs), which include human embryonic stem cells (hESCs) and human induced pluripotent stem cells (hiPSCs), are powerful tools to study developmental biology and mechanisms underlying pathological processes. A pertinent application of hPSCs is in recapitulating the organogenesis of human bone. The human skeleton originates from three distinct embryonic lineages: the frontal skull and facial bones arise from the neural crest and the remaining skeleton from the paraxial and lateral plate mesoderm.¹ These differences in the developmental origins of bone are captured by diseases that affect specific bone types. Examples include Robinow syndrome—which affects the vertebrae of the axial skeleton—and acheiropodia—which causes truncation of the upper and lower extremities of the appendicular skeleton.² There are also diseases isolated to craniofacial bones, such as Muenke syndrome. In an *in vivo* study utilizing a Muenke syndrome mouse model, authors reported significant shortening of presphenoid and basi-sphenoid bones, whereas basioccipital bones were unaffected. Through fate mapping studies, McBratney-Owen et al demonstrated that these affected bones are neural-crest derived, while the basioccipital bone is paraxial mesoderm in origin.³ Further investigation of disorders affecting particular bone types would be greatly informative of bone development and disease mechanisms, making the derivation of lineage-specific osteogenic progenitors (OPs) from hPSCs highly beneficial. This study aimed to generate three subpopulations of OPs derived from paraxial mesoderm-like (PM) cells, lateral plate mesoderm-like (LP) cells, and neural crest-like (NC) cells.

Differentiation of hPSCs directly into OPs has been reported by several studies that employ various differentiation conditions and selection criteria for purifying cell populations.⁴⁻⁷ However, the embryonic germ layer from which they originated is often not described. Instead, two-step differentiation protocols broadly refer to osteogenic precursors as “mesenchymal stem cell-like” populations. This is a major limitation in recapitulating early developmental

Significance statement

Given that the human skeleton arises from different embryonic origins, modeling early bone development with human pluripotent stem cells benefits from a method of lineage-specific derivation. This study proposes a stepwise differentiation protocol toward paraxial mesoderm-, lateral plate mesoderm-, and neural crest-derived osteogenic progenitors with characterization at each stage. This approach establishes the utility of pluripotent stem cells in recapitulating osteogenesis and potential application in disease modeling. Our study's identification of transcriptomic signatures of each subpopulation reveals, for the first time, high FGF1 levels in neural crest-derived osteoprogenitors and its influence on RUNX2, a finding that suggests its potential role in craniofacial diseases.

stages of bone and reducing heterogeneity in cell populations. Previous work that attempts to address this shortcoming perform stepwise differentiation of hPSCs into osteoprogenitors in serum- and feeder-free conditions^{1,8,9} but still do not generate all three OP lineages, perform *in vivo* transplantation to confirm true osteogenic capacity, and/or describe transcriptomic patterns. As a result, the characterization of the differences among hPSC-derived OPs remains incomplete. To address these gaps, our study presents a method of stepwise differentiation of lineage-specific OPs from hiPSC- and hESC-derived PM, LP, and NC cells using chemically defined and serum-free culture conditions. We performed cell sorting coupled with gene expression analysis to optimize induction purity and employed a novel hESC-RUNX2-YFP reporter cell line that allowed the identification of the earliest OPs.^{6,10} With our differentiation system, we characterized differences among transcriptomic patterns and highlight key markers of the three cell populations.

We also report the presence of high levels of fibroblast growth factor 1 (FGF1), an important signaling molecule in bone-related processes, in neural crest-derived OPs. The 23 members of the fibroblast growth factor (FGF) family bind to fibroblast growth factor receptors (FGFRs), leading to receptor dimerization and trans-autophosphorylation of the kinase domain.¹¹ Together, FGF-FGFRs play essential developmental and homeostatic roles in the skeleton by regulating chondrocyte and osteoblast differentiation and proliferation.¹² Indeed, aberrancy in their signaling cascades causes various well-established skeletal diseases, such as achondroplasia from FGFR3 gain-of-function mutations.¹³ FGFR signal transduction is comprised of four major pathways: phosphoinositide-3-kinase/AKT (PI3K/AKT), phospholipase C γ (PLC γ), signal transducer and activator of transcription (STAT), and the RAS/mitogen-activated protein kinase (MAPK) pathways.¹⁴ MAPK is the predominant downstream pathway of activated FGFRs, modulating cell proliferation and, in certain contexts, differentiation.¹⁵ Therefore, to explore the role of endogenous FGF1 in NC-OPs and its potential influence on bone, we investigated its effects on Runt-related transcription factor 2 (RUNX2), a master transcription factor for osteoblast differentiation.¹⁶ We hypothesized that FGF1 regulates RUNX2 at multiple levels, with evidence implicating MAPK involvement, specifically extracellular signal-regulated kinases 1 and 2 (ERK1/2 or MAPK1/3). Taken together, our study validates hPSCs as a powerful tool to model bone development and draws attention to FGF1 as a protein of interest for future studies on disorders of neural crest-derived structures.

2 | MATERIALS AND METHODS

2.1 | Cell lines

NCRM-5 hiPSCs were derived from male CD34⁺ cord blood and reprogrammed by the NIH Center for Regenerative Medicine (<https://commonfund.nih.gov/stemcells/lines#RMP-generated%20iPSC%20lines>). hESC line H9 (WiCell, Madison, Wisconsin) transfected with a RUNX2-YFP reporter (hESC-RUNX2-YFP) was produced by the Kaufman laboratory at the University of Minnesota⁶ and was maintained as undifferentiated cells as previously described.⁶ hESC-RUNX2-YFP cells used to report differentiation into osteoprogenitors (OPs) were previously described.¹⁰

2.2 | hPSC culture and differentiation

Before stepwise differentiation into OPs, hiPSCs and hESC-RUNX2-YFP were replated into human xeno-free vitronectin XF (STEMCELL Technologies, Vancouver, BC, Canada) precoated wells at 10 μ g/mL in Essential 8 Media (E8) (ThermoFisher Scientific, Waltham, Massachusetts). For primitive streak-like (PS) cell differentiation, E8 media was replaced with basal differentiation media (STEMdiff APEL; STEMCELL Technologies) supplemented with 5 μ M GSKi (CHIR99021) (Stemgent, Lexington, Massachusetts) for 24 hours as previously

reported.¹⁷ For further differentiation into PM cells, PS cells were kept in basal differentiation media supplemented with 10 μ M TGF- β inhibitor (SB431542) (Sigma-Aldrich, St. Louis, Missouri) and BMP inhibitor (LDN193189) (Axon MEDCHEM, Reston, Virginia) for 6 days. For LP cell differentiation, PS cells were kept in basal differentiation media supplemented with 25 ng/mL recombinant human bone morphogenetic protein 4 (rhBMP4) (Peprotech, Rocky Hill, New Jersey) and recombinant human vascular endothelial cell growth factor (rhVEGF) (ThermoFisher Scientific) for 6 days. NC differentiation was accomplished in basal differentiation medium with 10 μ M SB431542 and 1 μ M GSKi for 6 days as previously reported.¹⁷

For osteogenic commitment, PM, LP, and NC cells were kept in the osteogenic basal medium (1% P/S, 1% MEM-NEAA, 2 mM L-Glutamine in α -MEM [ThermoFisher Scientific], 10% Knockout Serum Replacer [KOSR], 50 μ g/mL ascorbic acid, 10 mM β -glycerophosphate and 100 nM dexamethasone) supplemented with osteogenic mediators: 100 ng/mL BMP2, 40 ng/mL FGF9, 4 nM rapamycin (all from ThermoFisher Scientific) and 0.5 μ g/mL Wnt3a (Creative Biomart, Shirley, New York) for 6 days. Subsequently, differentiation was continued with osteogenic medium without osteogenic mediators until day 28 from the start of differentiation. The medium was changed every 3 days. Cells were cultured at 37°C in 5% CO₂ at 95% humidity. Bone marrow stromal cells (BMSCs) grown in osteogenic medium supplemented with 20% FBS were taken as positive controls. Undifferentiated hPSCs were taken as the negative controls.

2.3 | Real-time reverse-transcription polymerase chain reaction

Real-time reverse-transcription polymerase chain reaction (RT-PCR) analysis was done as previously described.¹⁰ Briefly, total RNA was extracted using Qiagen RNeasy Mini Kit (Qiagen, Valencia, California) and 1 μ g of RNA was reverse transcribed into cDNA using SuperScript II Reverse Transcriptase (ThermoFisher Scientific), based on the manufacturer's instructions. Quantitative real-time RT-PCR was performed using 150 ng cDNA product with SYBR Green PCR Master Mix (Qiagen) in 25 μ L per PCR reaction according to the recommended conditions as previously described.¹⁰ The genes amplified are listed in Table S1. The level of the target genes was correlated with the standard concentrations and normalized by GAPDH levels as an endogenous reference.

2.4 | Flow cytometric analysis and cell sorting

A single-cell suspension of undifferentiated and differentiated cells was prepared as previously described⁶ and evaluated for RUNX2 and surface proteins using the fluorescence-activated cell-sorting facility (FACSCalibur, BD, San Jose, California) in the NIDCR Combined Technical Research Core. Flow cytometry data were analyzed with the FlowJo software (Tree Star, Ashland, Oregon). Antibodies are listed in Table S2.

2.5 | Immunofluorescence staining, in situ hybridization, Immunohistochemistry, and staining

Immunofluorescence staining was performed as described previously.¹⁹ Briefly, cells were fixed with 2% formaldehyde, washed twice with PBS, and incubated with primary antibodies for 1 hour at room temperature. Then, cells were washed three times and incubated with secondary antibodies diluted 1:100 for 1 hour at room temperature and visualized by confocal microscopy. In situ hybridization was performed according to the manufacturer's recommendation (#A001K.9905, Rembrandt Universal Dish & AP Detection Kit). Briefly, the detection of human cells in the bone formed in vivo was assessed by in situ hybridizations for human-specific *ALU* repetitive DNA sequences. Immunohistochemistry was performed as previously reported.²⁰ Briefly, the sections were deparaffinized and antigens retrieved with Uni-Trieve (Innovex Biosciences, Richmond, California). Sections were blocked for 20 minutes in blocking buffer (1% BSA, 2% donkey serum, 0.1% Triton X100 in PBS). Incubations with primary antibody were done overnight at 4°C in blocking buffer. Secondary antibodies were incubated at 1:400 dilution for 1.5 hours at room temperature. Nonimmune immunoglobulins of the same isotype were used as negative controls. For H&E staining, sections of in vivo transplants were stained with H&E or toluidine blue and imaged with bright-field microscopy as reported previously.⁷

2.6 | Enzyme-linked immunosorbent assay, siRNA knockdown, and western blot analysis

FGF1 was quantified using Human FGF1 SimpleStep ELISA kit (Abcam, Cambridge, Massachusetts) according to the manufacturer's instructions. Briefly, the culture medium was collected over 5 days for all OPs and centrifuged at 2000g for 10 minutes. The total protein concentration of the supernatant was quantified using the Pierce BCA Protein Assay Kit (ThermoFisher Scientific). Samples and standards were loaded in duplicate in a 96-well plate coated with an anti-tag antibody, along with capture and detector antibodies. After a 1-hour incubation at room temperature, wells were washed three times and 3,3',5,5'-tetramethylbenzidine substrate was added for 10 minutes. Stop Solution was added, and optical density was measured at 450 nm using a Varioskan LUX microplate reader (ThermoFisher Scientific). FGF1 knockdown was performed with FGF1 Silencer Predesigned siRNA (ThermoFisher Scientific). siRNA and the negative control were diluted in Opti-MEM I reduced serum medium (ThermoFisher Scientific) and added to Lipofectamine RNAiMAX transfection reagent (ThermoFisher Scientific). After incubation for 5 minutes at room temperature, the siRNA-lipid complex was added to NC-OPs cultured in 6-well plates at 37°C in 5% CO₂ and 95% humidity for 72 hours. The efficiency of knockdown was assessed through ELISA. For immunoblot analysis, the protein was extracted from NC-OPs with Extraction Buffer 5× PTR (Abcam), and total protein was measured with BCA assay. 50 µg of total protein was used for SDS-PAGE and transferred to nitrocellulose membrane. Erk1/2

was detected using p44/42 MAPK (Erk1/2) rabbit mAb (Cell Signaling Technology, Danvers, Massachusetts) diluted 1:1000 and β-actin rabbit pAb (Cell Signaling Technology) diluted 1:5000 served as housekeeping.

2.7 | Subcutaneous transplants in mice

The use of deidentified human samples was exempted by the NIH Office of Human Subjects Research Protection (exemptions #393 and #13255). For transplant experiments, mice were approximately 8 weeks old, 2530 g in weight and immunodeficient (NSG, NOD.Cg-Prkdc<scid>Il2rg<tm1Wjl>/SzJ, The Jackson Laboratory, Farmington, Connecticut). Transplants were constructed that contained approximately 2 million cells attached to 40 mg of the ceramic scaffold (Attrax [ceramic only], Nuvasive, San Diego, California). The anesthetized mouse was placed in ventral recumbency and the surgical area (dorsal surface) was prepared by alternating wipes of betadine and 70% ethanol three times. Autoclaved scalpel blades and scissors were used to make a 3-cm longitudinal incision in the skin. The tips of the scissors were used to make a pocket for the transplant via blunt dissection. Sterile scaffolds (40 mg) seeded with donor cells were placed into each subcutaneous pocket. The incision was closed with an autoclip and surgical tissue adhesive. The incision site was dried with sterile gauze.

2.8 | cDNA/library preparation, RNA sequencing, and analysis

Total RNA was reverse transcribed by Superscript IV (Invitrogen, Carlsbad, California) using template switching oligo and oligo dT primers followed by amplification of the second strand cDNA with LongAmp Taq polymerase (New England Biolabs, Ipswich, Massachusetts). Libraries were prepared using the Nextera XT kit (Illumina, San Diego, California), individually barcoded, pooled to a 2 nM final pooled concentration, and sequenced on a NextSeq500 instrument (Illumina) using either the 75 single-end or the 75 × 75 paired-end mode. After sequencing, the base-called demultiplexed (fastq) read qualities were determined using FastQC (v0.11.2), aligned to the GENCODE v25 human genome (GRCh38.p7), and gene counts were generated using STAR (v2.5.2a).²¹ Postalignment qualities were generated with QoRTS (v 1.1.6).²² An expression matrix of raw gene counts was generated using R and filtered to remove low count genes (less than five reads in at least one sample). The filtered expression matrix was used to generate a list of differentially expressed genes between the sample groups using three statistical methods: DESeq2,²³ EdgeR,²⁴ and Limma-voom.²⁵

2.9 | Statistical analysis

Each experiment was repeated independently twice with three biological replicates within each experiment unless stated otherwise in the figure legends. Results were presented as mean ± SEM. Statistical

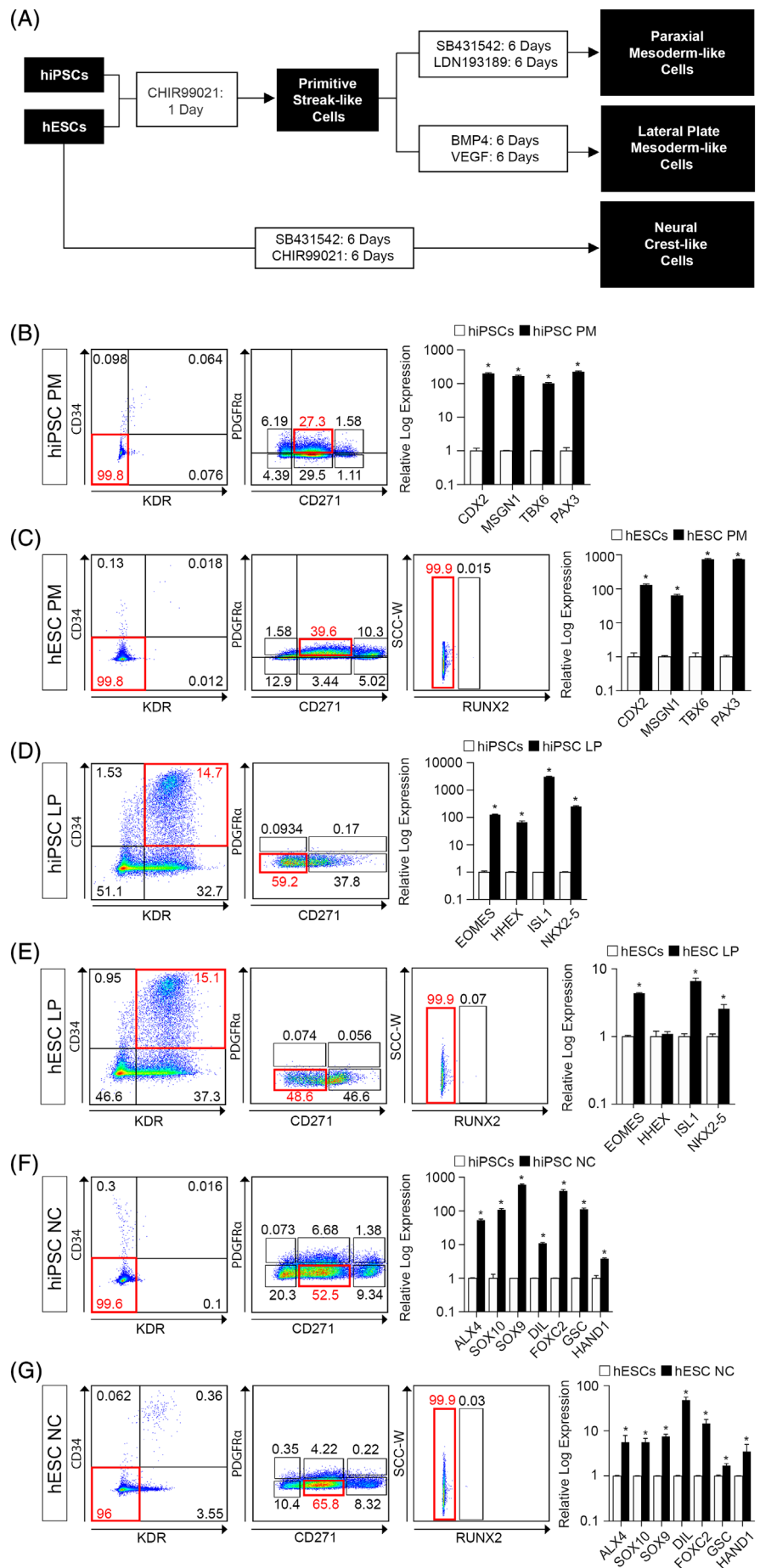


FIGURE 1 Stepwise differentiation of hPSCs into paraxial mesoderm-like (PM) cells, lateral plate mesoderm-like (LP) cells, and neural crest-like (NC) cells. A, Schematic diagram of stepwise differentiation and culture conditions of hiPSCs and hESCs toward primitive streak-like (PS) cells, PM cells, LP cells, and NC cells. B, Flow cytometric analysis showing marker expression of PM cells derived from hiPSCs and sorting for KDR⁻/CD34⁻/CD271^{dim}/PDGFR α ⁺ cells. C, Flow cytometric analysis showing the marker expression of PM cells derived from hESCs and sorting for KDR⁻/CD34⁻/CD271^{dim}/PDGFR α ⁺/RUNX2⁻. D, Flow cytometric analysis of marker expression of hiPSC-derived LP cells and sorting for CD34⁺/KDR⁺/PDGFR α ⁻/CD271⁻ cells. E, Flow cytometric analysis of marker expression of hESC-derived LP cells and sorting for CD34⁺/KDR⁺/PDGFR α ⁻/CD271⁻/RUNX2⁻ cells. F, Flow cytometric analysis showing marker expression of hiPSC-derived NC cells and sorting for CD34⁻/KDR⁻/PDGFR α ⁻/CD271^{dim} cells. (G) Flow cytometric analysis showing marker expression of hESC-derived NC cells and sorting for CD34⁻/KDR⁻/PDGFR α ⁻/CD271^{dim}/RUNX2⁻ cells. (B-G) Postsorted qRT-PCR analysis for PM, LP, and NC markers (mean \pm SEM, n = 3 biological replicates, *P < .05 vs respective undifferentiated hPSCs). Differentiation efficiencies (%) are shown, with sorted population in red text. PM, LP, and NC analyses were done on day 7 of differentiation

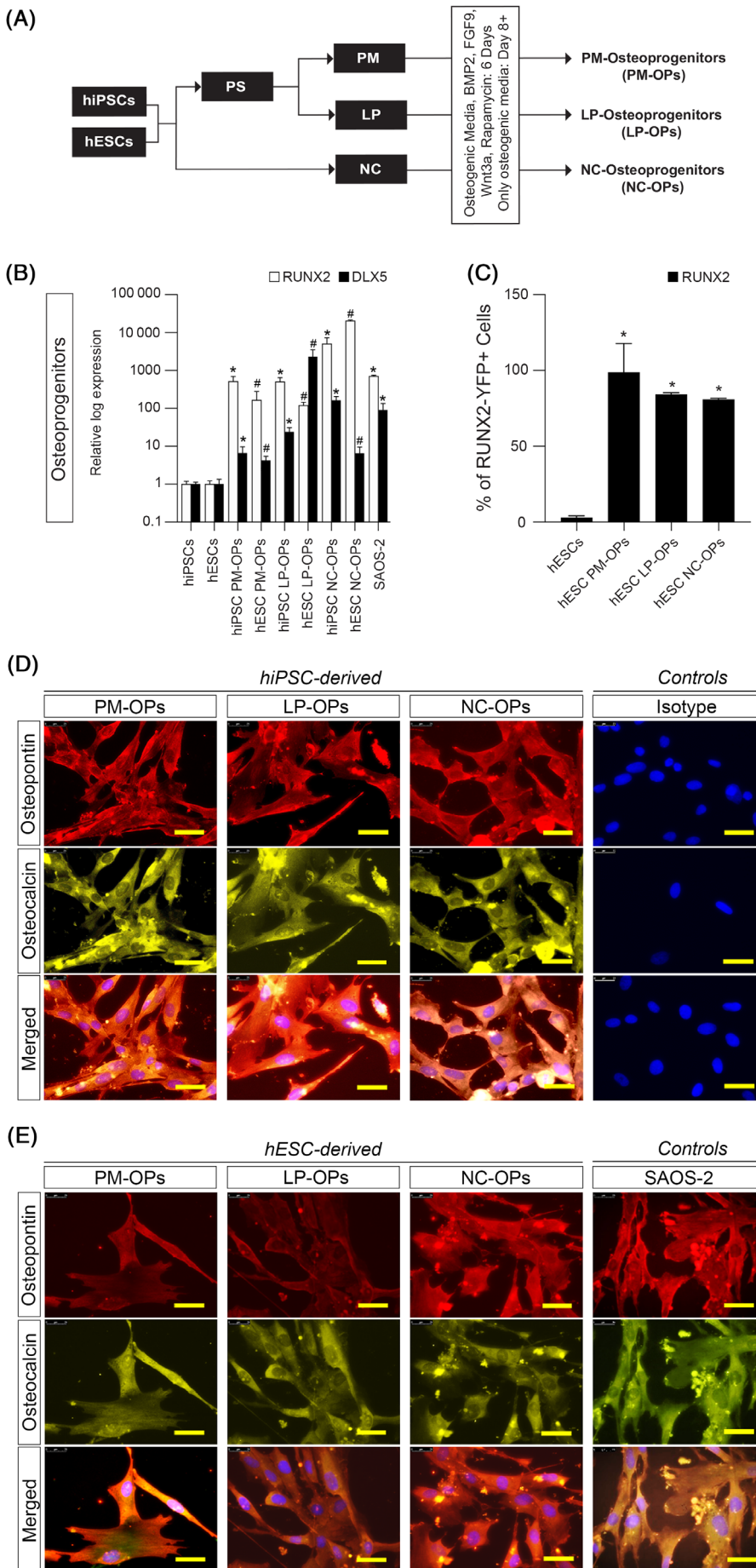


FIGURE 2 In vitro characterization of hPSC-derived lineage-specific osteogenic progenitor (OP) cells. A, Schematic diagram showing stepwise differentiation and culture conditions of PM, LP, and NC cells into their respective OP cells. B, Quantitative mRNA analysis of osteogenic markers, *RUNX2* and *DLX5* (mean \pm SEM, $n = 3$ biological replicates, $*P < .05$ vs hiPSCs, $\#P < .05$ vs hESCs). C, Analysis of osteogenic differentiation efficiency by flow cytometry of *RUNX2*-YFP expression of hESC-derived OPs (mean \pm SEM, $n = 3$ biological replicates, $*P < .05$ vs hESCs). D and E, Immunofluorescence staining for *OSTEOPONTIN* and *OSTEOCALCIN* in OPs derived from their respective hPSC. Isotype was negative control. SAOS-2 was used as a positive control. Analyses were done on 28 days after osteogenic differentiation. Scale bar = 100 μ m

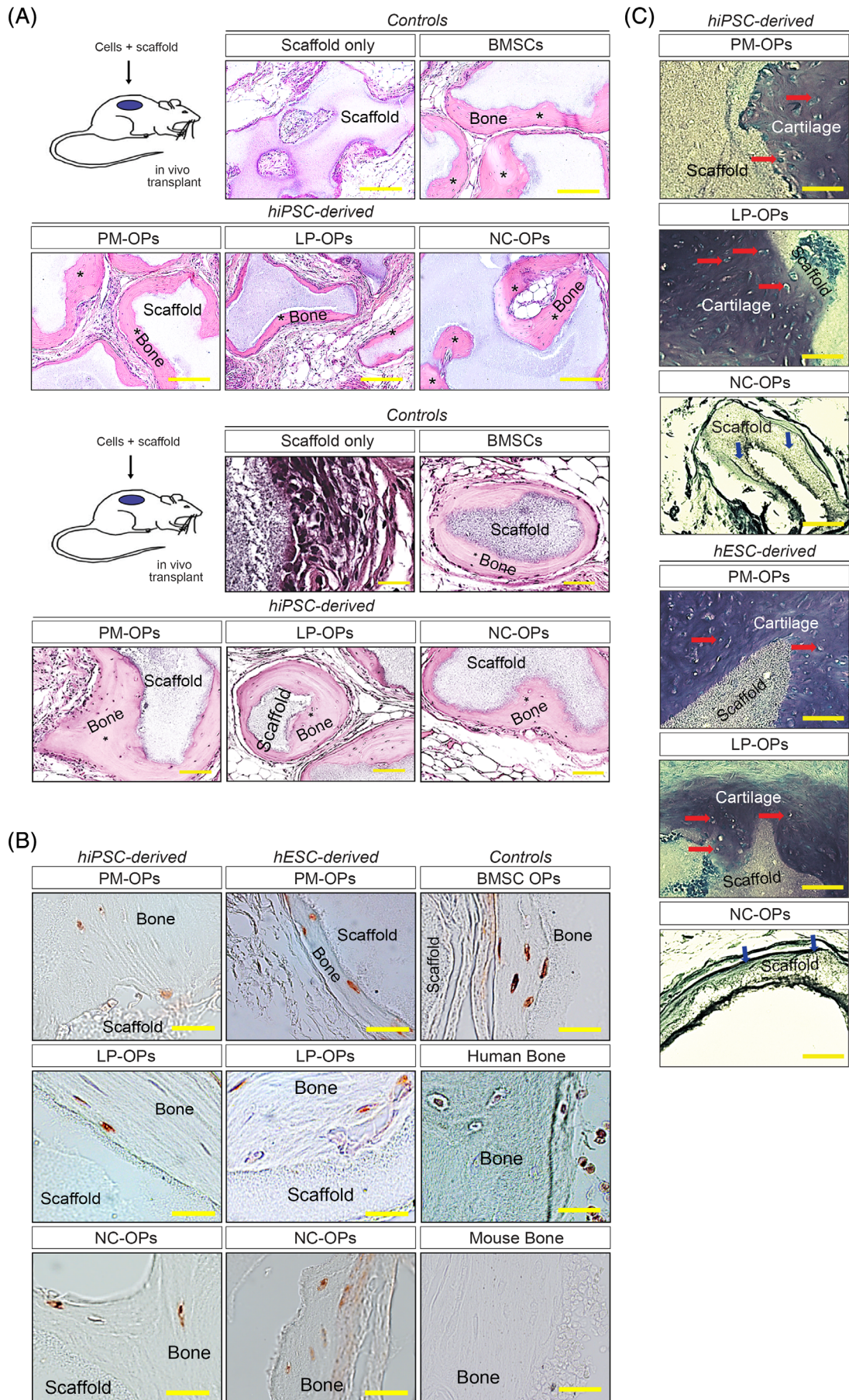


FIGURE 3 Legend on next page.

analysis was performed using GraphPad Prism (GraphPad Software, La Jolla, California). One-way or two-way analysis of variance was used for multiple comparisons. *P* values were calculated by one-tailed Student's *t* test, and significant differences were defined by *P* < .05.

3 | RESULTS

3.1 | Stepwise differentiation of OPs from hPSCs in vitro

To mimic gastrulation during which the primitive streak (PS) forms, hPSCs were differentiated into PS using the GSK inhibitor, CHIR99021, as demonstrated previously^{26,27} (Figure 1A). hPSC-derived PS cells showed significantly higher expression of primitive streak markers (*BRACHYURY* (*T*), *MESP1*, *MIXL1*, and *FOXF1*) at the mRNA level compared with undifferentiated hPSCs (Figure S1A, B). *T*, *MIXL1*, and *MESP1* are early, reliable markers of gastrulation²⁸⁻³⁰; *FOXF1* expression signifies the development of mesoderm during the late primitive streak stage.³¹

Given that the primitive streak gives rise to paraxial mesoderm, lateral plate mesoderm, and definitive endoderm,³² PS cells were differentiated into PM using the BMP inhibitor, LDN193189, and TGF- β inhibitor, SB431542 (Figure 1A), a protocol modified from Tan et al (2013). Gene expression analysis of PM cells revealed higher expression of paraxial mesoderm markers (*TBX6*, *PDGFR α*) compared with primitive streak (*T*, *MIXL1*), lateral plate (*CD34*, *KDR*), endoderm (*FOXA2*) and pluripotent (*OCT4*) markers (Figure S2A). *PDGFR α* has been used as a key marker of paraxial mesoderm,³³⁻³⁵ and in vivo studies have shown that *TBX6* is expressed in nascent and maturing paraxial mesoderm.³⁶ *FOXA2* specifies endoderm in the posterior epiblast³⁷ and *OCT4* is expressed in embryonic stem and germ cells.³⁸ Because *CD34* and *KDR* are established markers for lateral plate mesoderm³⁹⁻⁴¹, PM cells were enriched by sorting for *KDR⁻/CD34⁻* phenotype and subsequently divided into *CD271^{high}/PDGFR α ⁺* and *CD271^{dim}/PDGFR α ⁺* subpopulations. BMSCs sourced from mesoderm-derived bone, such as the iliac crest, reliably express *CD271*.^{42,43} The *CD271^{dim}/PDGFR α ⁺* population expressed higher paraxial mesoderm markers, *TBX6* and *PAX3* (Figure S2B), and was further characterized. Cells of this phenotype had significantly higher levels of paraxial mesoderm markers (*CDX2*, *MSGN1*, *TBX6*, and *PAX3*) compared with undifferentiated hPSCs (Figure 1B,C). *CDX2* is essential for PM-derived axial bone embryogenesis.⁴⁴ *PAX3* and *MESOGENIN 1* (*MSGN1*) are master regulators of paraxial mesoderm.⁴⁵ Because *RUNX2* is the master transcription factor for osteogenic

commitment,¹⁶ *RUNX2*-YFP expression was measured to detect osteogenic commitment, of which there was none (Figure 1C).

hPSC-derived PS cells were also differentiated into LP cells with BMP4 and VEGF, using a protocol developed by Tan et al¹⁷ (Figure 1A) and corroborated by others.⁴⁶ LP cells had higher expression of known lateral plate markers (*CD34*, *KDR*) compared with the primitive streak, paraxial mesoderm, endoderm, and pluripotent markers (Figure S3A). To confirm an enriched LP population, cells were sorted into *KDR⁺/CD34⁻/CD271⁻/PDGFR α ⁻*, *KDR⁺/CD34⁺/CD271⁻/PDGFR α ⁻* and *KDR⁻/CD34⁺/CD271⁻/PDGFR α ⁻* populations. The *KDR⁺/CD34⁺/CD271⁻/PDGFR α ⁻* subpopulation showed the highest expression of the LP marker, *EOMES*, compared with the other two populations (Figure S3B). *EOMES* plays a crucial role in early gastrulation, and its deficiency results in loss of LP formation.⁴⁷ Therefore, enriched LP cells (*KDR⁺/CD34⁺/CD271⁻/PDGFR α ⁻*) were further analyzed for LP lineage markers (*EOMES*, *HHEX*, *NKX2-5*, and *ISL1*) (Figure 1D,E). Activated by *HHEX*,⁴⁸ *NKX2-5* is reported to be a key modulator of LP maturation.⁴⁹ Additionally, *ISL1* is reported to be upstream of the sonic hedgehog pathway for LP differentiation.⁵⁰ *RUNX2*-YFP expression in hESC-derived LP cells was analyzed and confirmed to be absent (Figure 1E).

NC cells were differentiated directly from hPSCs by using the protocol reported by Fukuta et al,¹⁷ which includes both TGF- β and GSK inhibitors (Figure 1A). Subsequently, the enrichment of cells was accomplished by sorting for *KDR⁻/CD34⁻. CD271* was also used as part of our selection criteria, as it is a known marker for neural crest cells.⁵¹ The *KDR⁻/CD34⁻/CD271^{dim}/PDGFR α ⁻* cells expressed higher neural crest markers (*ALX4*, *SOX10*) compared with *KDR⁻/CD34⁻/CD271^{high}/PDGFR α ⁻* cells (Figure S4A). *ALX4* is upregulated in NC, and its mutation is associated with craniofacial disorders.⁵² *SOX10* appears during neural crest migration and regulates both neural crest survival and differentiation.⁵³ Therefore, *KDR⁻/CD34⁻/CD271^{dim}/PDGFR α ⁻* cells were sorted to achieve a further enriched population of NC cells. NC cells were also characterized for cranial neural crest markers (*ALX4*, *GSC*), neural crest specifier genes (*SOX10*, *SOX9*), and neural plate border genes (*DIL*, *FOXC2*, and *HAND1*) to confirm the neural crest lineage (Figure 1F, G); all genes were expressed significantly higher than undifferentiated hPSCs. *GSC* is required during embryogenesis and normal formation of craniofacial structures.⁵⁴⁻⁵⁶ *SOX9* precedes markers of migratory neural crest.⁵⁷ *DIL* acts in the dorsal part of the neural tube.^{58,59} *FOXC2*⁶⁰ and *HEART AND NEURAL CREST DERIVATIVES EXPRESSED 1* (*HAND1*) expression has been reported in neural crest cells, with the latter involved in *RUNX2*-IHH-regulated endochondral ossification.⁶¹ The hESC-derived NC-enriched population did not display signs of osteogenic differentiation (Figure 1G).

FIGURE 3 In vivo characterization of hPSC-derived lineage-specific osteogenic cells. A, H&E staining of subcutaneous transplants formed by hPSC-derived PM-OPs, LP-OPs, and NC-OPs in immunocompromised mice. Scaffold without cells served as the negative control and transplanted BMSCs as a positive control. Transplants were analyzed at 16 weeks. Scale bar = 100 μ m. B, In situ hybridization for human-specific *ALU* DNA sequences in calcified tissue formed by hPSC-derived OPs transplanted with scaffold into immunocompromised mice. Transplants with BMSCs and human bone were positive controls. Negative control was a normal mouse bone. Transplants were harvested and analyzed at 16 weeks. Scale bar = 100 μ m. C, Toluidine blue staining of transplants with hPSC-derived OPs with the scaffold. Red arrows indicate hypertrophic chondrocytes, and blue arrows indicate bone. Analyses were performed at 8 weeks. Scale bar = 100 μ m

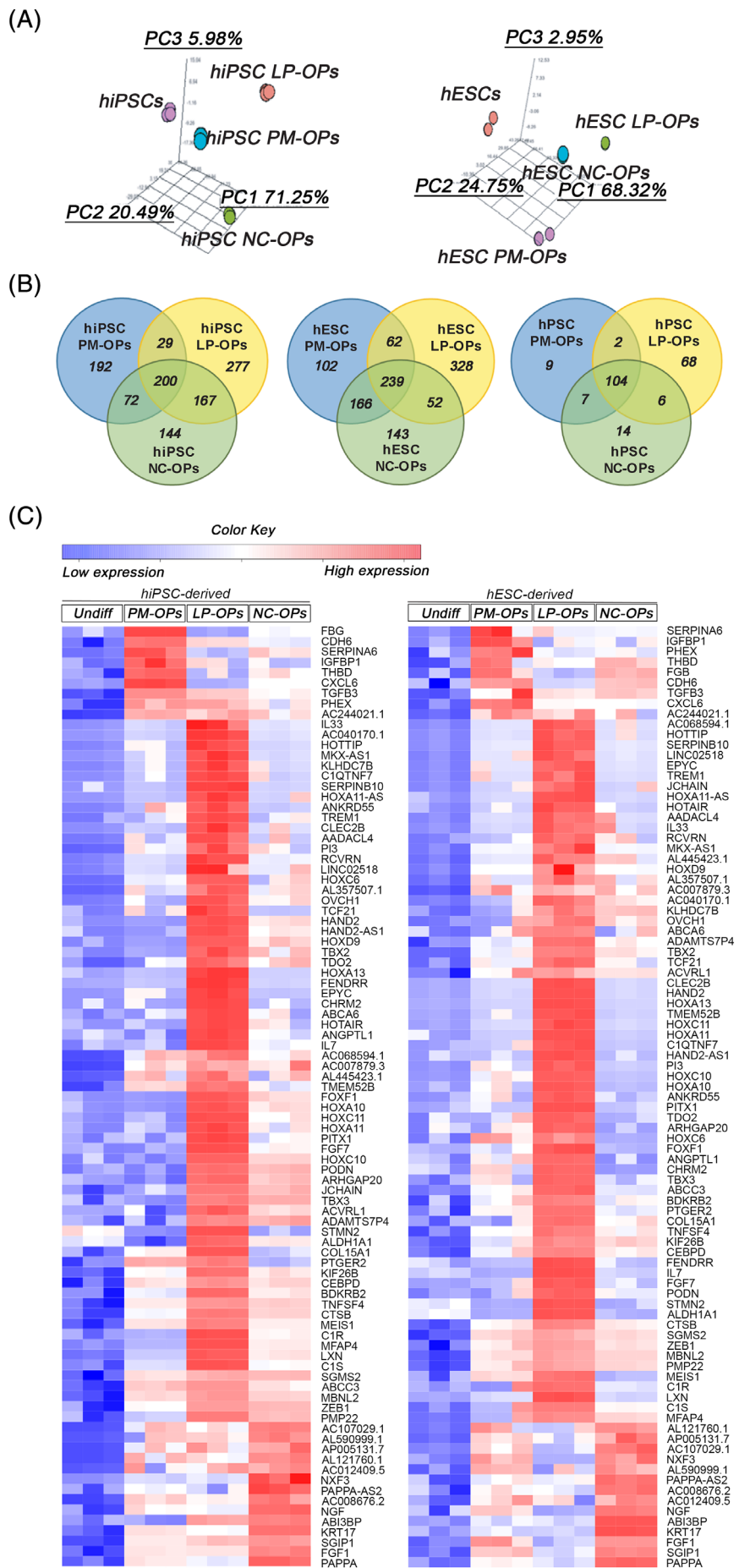


FIGURE 4 Transcriptomic patterns of PM-OPs, LP-OPs, and NC-OPs. A, Principal component analysis plot showing OPs derived from hiPSCs and hESCs. B, Venn diagrams showing unique and shared genes expressed by PM-OPs, LP-OPs, and NC-OPs derived from hiPSCs or hESCs or combined. C, Heat maps showing genes expressed exclusively by PM-OPs, LP-OPs, and NC-OPs derived from both hiPSC and hESC lines (log2 transformed normalized expression). Analyses were performed 28 days after beginning osteogenic differentiation. After PCA, genes selected for further analysis were expressed at least 5.5x log-fold higher than expression levels in undifferentiated cells

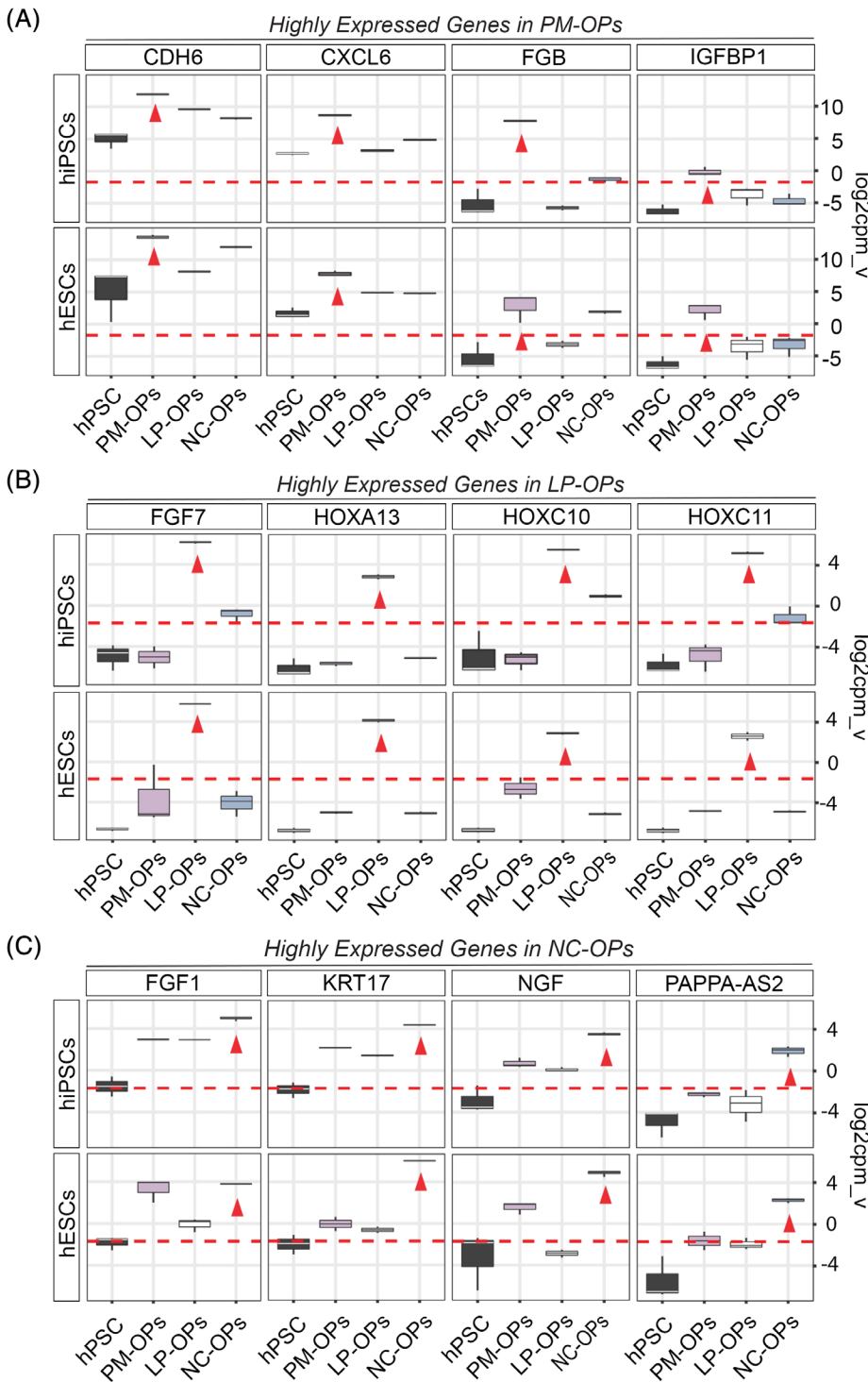


FIGURE 5 Genes most expressed in PM-OPs, LP-OPs, and NC-OPs. A, Box plot of the top 4 genes expressed by PM-OPs. B, Box plot of the top 4 genes expressed by LP-OPs. C, Box plot of the top 4 genes expressed by NC-OPs. Analyses were performed 28 days after beginning osteogenic differentiation. Red arrowhead: $>5.5\times$ log-fold higher vs hPSCs. Dotted red line: less than five reads in at least one sample (mean \pm SEM, $n = 3$ biological replicates)

3.2 | Derivation of PM-OPs, LP-OPs, and NC-OPs in a serum-free microenvironment

hPSC-derived progenitors were further differentiated into three OP groups in serum-free medium as previously reported¹⁰: PM-OPs, LP-OPs, and NC-OPs (Figure 2A). These OPs expressed significantly higher levels of *RUNX2* and *DLX5* compared with respective undifferentiated hPSCs (Figure 2B). *DLX5* is a homeobox protein that drives osteoblast differentiation.⁶² Using flow cytometry, a significantly higher

percentage of *RUNX2*-YFP-positive hESC-derived OPs compared with undifferentiated hESCs confirms high osteogenic differentiation efficiency (Figure 2C). PM-OPs, LP-OPs, and NC-OPs derived from both iPSCs and hESCs demonstrated positive staining for key bone matrix proteins *OSTEOPONTIN* and *OSTEOCALCIN* at Day 28 (Figure 2D,E). SAOS-2, an osteosarcoma cell line, served as a positive control.

The osteogenic fate of OPs was validated by subcutaneous transplantation of OPs attached to ceramic particles into mice. OPs and BMSCs (positive control) formed bone at 16 weeks (Figure 3A), which

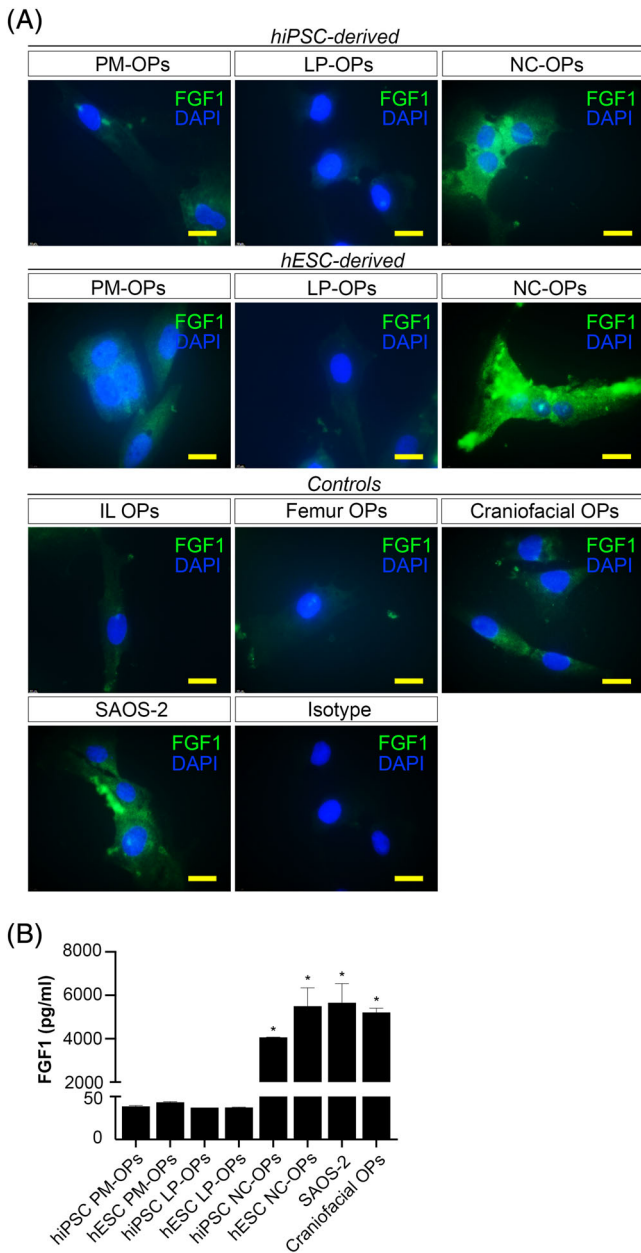


FIGURE 6 High FGF1 expression by NC-OPs in vitro and in vivo. A, Immunofluorescence staining for FGF1 expression in PM-OPs, LP-OPs, and NC-OPs. Isotype control was taken as a negative control. BMSCs derived from iliac crest, femur, and a craniofacial site were osteogenically differentiated and taken as positive controls. 4',6'-diamidino-2-phenylindole (DAPI) was used as a counterstain. Scale = 100 μ m. Analyses were done 28 days after the start of osteogenic differentiation. B, Enzyme-linked immunosorbent assay for FGF1 in culture medium for PM-, LP-, and NC-OPs, with SAOS-2 as the positive control (mean \pm SD, n = 2 biological replicates, *P < .05 vs PM-OPs and LP-OPs)

was confirmed to be of human origin by in situ hybridization probes for human-specific ALU DNA sequences (Figure 3B). PM-OPs and LP-OPs also formed chondrocytes after 8 weeks of transplants (Figure 3C), which may represent the cartilage intermediate in endochondral ossification that occurs in axial and appendicular skeleton.⁶³

On the other hand, evidence of chondrogenic ossification in NC-OPs was not found (Figure 3C). In contrast with endochondral ossification, intramembranous ossification does not include a cartilage template. Instead, the flat bones of the calvaria form from neural crest-derived OPs that proliferate and condense into compact nodules containing osteoblasts, which deposit osteoid matrix that later calcifies.⁶³ Overall, histological data indicates that OPs may form bone in vivo in a process similar to native bone development. However, further investigation is required for confirmation.

3.3 | The unique transcriptomic patterns of PM-OPs, LP-OPs, and NC-OPs

To describe differences in lineage-specific transcriptomic patterns, principal component analysis (PCA) was performed using the top 500 most variable genes (Figure 4A). Variation was appreciated among the three populations of OPs independent of the cell line from which they were derived, with tight grouping among experimental replicates. Clear differences were also observed in transcriptional profiles of OPs across cell lines. Among hiPSC-derived OPs, the transcriptional profiles of LP- and NC-OPs were most dissimilar. On the other hand, among hESC-derived OPs, the transcriptional profile of LP- and PM-OPs were most dissimilar (Figure 4A).

To further characterize these differences, the signature transcriptomic patterns of PM-OPs, LP-OPs, and NC-OPs were analyzed. Any gene with at least a 5.5x log-fold or higher expression in OPs relative to their respective undifferentiated hPSCs was selected for signature transcriptomic pattern analysis. A total of 613 uniquely expressed genes in hiPSC-derived PM-OPs (192 genes), LP-OPs (277 genes), and NC-OPs (144 genes) were found (Figure 4B). A total of 573 uniquely expressed genes were found in hESC-RUNX2-YFP-derived PM-OPs (102 genes), LP-OPs (328 genes), and NC-OPs (143 genes) (Figure 4B). A list of genes shared between hiPSC- and hESC-derived OPs was compiled. Nine exclusive genes in PM-OPs (Figure 4B, Table S3), 68 in LP-OPs (Figure 4B, Table S4), and 14 in NC-OPs (Figure 4B, Table S5) were found. Also identified were genes shared between LP-OPs and PM-OPs (2 genes) (Table S6), PM-OPs and NC-OPs (7 genes) (Table S7), and NC-OPs and LP-OPs (6 genes) (Figure 4B, Table S8). Lastly, 104 genes were shared by all populations of OPs derived from both hiPSCs and hESCs (Figure S4B, Table S9). These highly expressed genes shared by OPs are displayed in heat maps (Figure 4C).

Next, we selected the four highest genes expressed in both hiPSC- and hESC-derived PM-OPs, LP-OPs, and NC-OPs compared with undifferentiated cells. Out of nine total common genes in PM-OPs, cadherin 6 (*CDH6*), chemokine C-X-C motif chemokine ligand 6 (*CXCL6*), fibrinogen beta chain (*FGB*), and insulin-like growth factor binding protein 1 (*IGFBP1*) were most expressed (Figure 5A). The highest expressed genes in LP-OPs were fibroblast growth factor 7 (*FGF7*) and a cluster of homeobox (*HOX*) family genes (*HOXA13*, *HOXC10*, and *HOXC11*) (Figure 5B). Fibroblast growth factor 1 (*FGF1*), keratinocyte 17 (*KRT17*), nerve growth factor (*NGF*) and pregnancy-associated plasma protein-A-antisense 2 (*PAPPA-AS2*) in NC-OPs were expressed the most (Figure 5C).

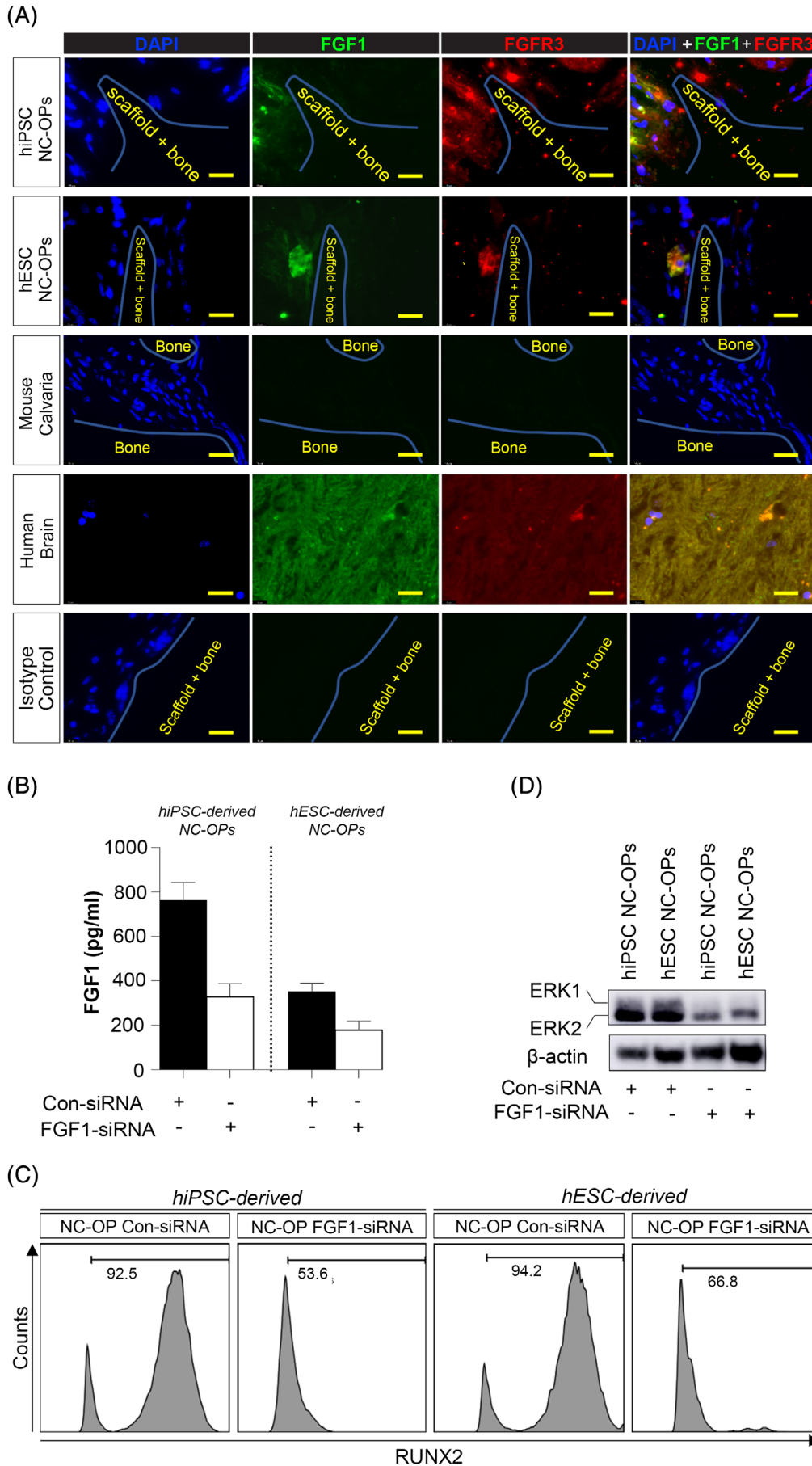


FIGURE 7 Legend on next page.

3.4 | Significantly higher FGF1 in NC-OPs

The link between craniofacial disorders and mutations in neural crest cells, coupled with the high expression of *FGF1* in NC-OPs, motivated deeper investigation into the role of *FGF1* in NC-OPs. Expression of *FGF1* in NC-OPs was confirmed using immunofluorescent imaging, with a high *FGF1* signal in NC-OPs compared with OPs of other lineages (Figure 6A). The data also showed more noticeable levels of *FGF1* in neural crest-derived BMSCs from the jawbone compared with those derived from the iliac crest and femur, which are both mesodermal in origin. Because *FGF1* is readily exported from cells by direct translocation across the cell membrane to serve paracrine and autocrine functions,⁶⁴ ELISA was performed on OP cell culture medium to quantify *FGF1* release. In support of the fluorescent signal patterns, NC-OPs released significantly more *FGF1* extracellularly compared to PM- and LP-OPs, which showed a more moderate release (Figure 6B). Craniofacial BMSCs had similarly high release and SAOS-2 served as the positive control. *FGF1* expression was then shown to be maintained *in vivo* by transplanted NC-OPs (Figure 7A). *FGF1* displayed affinity toward *FGFR3*, one potential receptor of *FGF1*, with a co-localizing signal (Figure 7A).⁶⁵ Human brain tissue was taken as a positive control for both ligand and receptor.^{66,67} The reaction of the human-specific antibody with the transplants compared with mouse calvaria served as a negative control.

3.5 | Inhibition of FGF1 reduces *RUNX2* expression

Studies have demonstrated various FGFs directly stimulate *RUNX2* expression and increase its binding to promoters, which in turn upregulate OP proliferation and differentiation into osteoblasts⁶⁸⁻⁷⁰. Therefore, to explore the potential role of *FGF1* in bone morphogenesis, NC-OPs were transfected with *FGF1*-siRNA, and its downstream effect on *RUNX2* was evaluated. Knockdown efficiency, assessed through ELISA of cell extracts, showed a mean decrease in *FGF1* of 57% and 49% in hiPSC-derived and hESC-derived NC-OPs, respectively, compared with corresponding scrambled siRNA control groups as negative controls (Figure 7B). Subsequent flow cytometric analysis showed marked decreases in *RUNX2* levels in NC-OPs when compared with controls (Figure 7C). Previously shown to be major molecules in the FGF-MAPK signaling pathway, *MAPK3* and *MAPK1* (*ERK1/2*) promote *RUNX2* transcriptional activity through phosphorylation and subsequent activation.^{71,72} Interestingly, western blot analysis showed a decrease in *ERK1/2* levels in NC-OPs after inhibition of *FGF1* (Figure 7D).

4 | DISCUSSION

This study recapitulated the development of lineage-specific osteogenic subpopulations by stepwise differentiation of hPSCs and identified their signature transcriptomic patterns. From PS to PM, LP, and NC, the success of the differentiation system was supported by the upregulated expression of corresponding lineage markers compared with the parental lines. Although we drew upon established differentiation protocols in this study, optimization was accomplished with the addition of cell sorting coupled with gene expression analysis using reliable markers and treatment modifications that enriched populations of interest. Of note, in PM differentiation, the initial approach was the treatment of PS cells with only SB431542, a TGF- β -mediated SMAD 2/4 inhibitor. TGF- β inhibition blocks endoderm differentiation and induces PM differentiation. However, high contamination with LP cells (*CD34*⁺/*KDR*⁺) was encountered. Therefore, in addition to TGF- β , PS cells were treated with the BMP-mediated SMAD 1/5 inhibitor, LDN193189. BMP is known to induce LP formation as opposed to PM.⁷³

The combined treatment successfully reduced LP cell contamination for more efficient derivation of an enriched population of PM cells. Interestingly, in contrast to the protocol set forth by Fukuta et al upon which ours is based, we encountered a higher expression of NC markers in *CD271*^{dim} subsets as opposed to *CD271*^{high}.¹⁷ This difference may be attributed to alternative choices in basal differentiation medium and sorting procedures. Nonetheless, higher *ALX4* and *SOX10* expression in our *CD271*^{dim} subset compared with that of *CD271*^{high} confirmed the purity of the NC population. In the final stages of differentiation, OPs clearly demonstrated osteogenic characteristics *in vitro* and *in vivo*, confirming their identity as bona fide OPs.

Lineage contamination is quite common in the differentiation of PS cells, preventing the study of lineage-specific transcriptomic patterns. Our lineage-specific differentiation allowed the characterization of separate OP subpopulations. To ensure that transcriptomic signatures are representative of OPs independent of the cell type from which they were derived, only highly expressed genes from both hiPSCs and hESCs were analyzed. Concerning the highest expressed PM-OP genes, it has been shown that *CDH6* is a target of TGF- β and is regulated by *RUNX2*.⁷⁴ *FIBRINOGEN* induces *RUNX2* activity through the SMAD1/5/8 signaling pathway.¹⁰ *CXCL6* has been reported to play an important role in bone formation during embryogenesis and in response to hormonal and mechanical stimuli.⁷⁵ Similarly, *IGFBP1* and its ligands, insulin-like growth factors, play key roles in bone metabolism.⁷⁶ In LP-OPs, *FGF7* is expressed in connective

FIGURE 7 FGF1 inhibition reduces *RUNX2* expression and *ERK1/2* signaling. A, Immunofluorescence staining for *FGF1* and *FGFR3* expression in transplants generated by hPSC-derived PM-OPs, LP-OPs, and NC-OPs. Mouse calvaria and antibody isotype controls were taken as negative controls. Human brain tissue was taken as positive control. DAPI was used as a counterstain. Scale = 100 μ m. Analyses were done on transplants harvested after 16 weeks. B, Measured using an enzyme-linked immunosorbent assay, *FGF1* knockdown efficiency for hPSC-derived NC-OPs compared to Con-siRNA (negative control) (mean \pm SD, n = 2 technical replicates). C, Flow cytometric analysis for *RUNX2* in NC-OPs treated with Con-siRNA and *FGF1*-siRNA. D, Western blot analysis of *ERK1*, *ERK2*, and β -actin (housekeeping) after NC-OP treatment with Con-siRNA and *FGF1*-siRNA

tissues and plays an essential role in regulating long bone development.⁷⁷ The cluster of HOX genes is known to provide cells with specific positional identities on the anterior-posterior axis.⁷⁷ They also have important roles in long bone embryogenesis.⁷⁸ Finally, KRT17 is expressed by NC-OPs in bone marrow stromal cells.⁷⁹ Osteoblast-secreted NGF stimulates nerve sprouting, which points to an interesting crosstalk between the skeletal and nervous systems.^{80,81} ANTI-SENSE A2 OF PAPPA (PAPPA-AS2) controls the upstream signaling pathway(s) during adipogenesis.⁸² Antisense transcripts cause cis-repression of transcription of their sense counterparts, which usually results in a negative correlation between the two transcriptional states.⁸³ This may play a role in the potential of NCs to give rise to tissues of ectodermal and mesodermal (connective) lineages.⁸⁰ When contextualized based on a particular OP's germ layer of origin, transcriptomic patterns meet expectations and further support the notion that OP differentiation remained faithful to lineage type.

Particularly interesting genes encountered from the transcriptomic analyses were those belonging to the FGF family. FGF pathways play critical roles in osteogenesis, mineral homeostasis, and ossification.^{12,64} In fact, several congenital bone diseases have been directly linked to mutations in FGFs and their receptors.⁸⁴ Demonstration of high expression of *FGF7* appears unique to LP-OPs, as other osteogenic progenitor types showed more modest expression. This phenotype is consistent with previous studies that have shown that *FGF7* appears in the mesodermal embryonic mesenchyme⁸⁵ and perichondrium, which helps give rise to the appendicular skeleton.^{86,87} Building upon the understanding of the tissue-specific expression of FGFs, we also presented, for the first time, that *FGF1* is found in high levels in NC-OPs. *FGF1* has been reported in diverse cell types, including preadipocytes and astrocytes.⁸⁸ However, to the best of our knowledge, there has not yet been evidence of endogenous *FGF1* activity in neural crest OPs. As such, this finding may have important implications regarding craniofacial bone disorders. *FGF2*, which possesses remarkable sequence homology to *FGF1*,⁸⁹ acts on neural crest cells in the development of murine frontal bone,⁸⁹ and dysfunction of the *FGF2* pathway can cause dysmorphic facial features. Mutation in the TGF- β type II receptor in mice, for example, causes downregulation of *FGF2* and compromised osteoblast differentiation of the orbital and calvarial components of the frontal bone primordium.⁸⁹ Notably, PM-OPs and LP-OPs also demonstrated high expression of *FGF1*. However, interestingly, immunofluorescent *FGF1* signal and extracellular protein levels were markedly higher in NC-OPs compared to other lineages. This discrepancy between RNA sequencing and immunofluorescent data may be due to post-transcriptional regulation, activity, and/or induction of *FGF1* in different tissue types.

Our study provided evidence that signaling induced by *FGF1* likely plays vital bone-related functions by modulating *RUNX2*. The significance of *RUNX2* is highlighted by mice harboring a homozygous mutation in *RUNX2*, which died immediately after birth and displayed a complete absence of bone formation and expression of bone markers.⁹⁰ *RUNX2* is also required for the maturation of prehypertrophic to hypertrophic chondrocytes during endochondral ossification.⁹¹ However, evidence that connects *FGF1* with *RUNX2* and describes the molecular mechanisms of regulation is limited. *RUNX2* is mediated through multiple mechanisms

associated with the various cascades initiated by FGFR. One study showed that treatment of osteoblast-like MC3T3-E1 cells with *FGF2* and *FGF4* strongly stimulated *RUNX2* expression,⁶⁸ with many lines of evidence pointing toward the PLC γ -protein kinase C pathway as the responsible route.^{68,92} Other studies have demonstrated that Smad-induced *junB* and p38 MAPK pathway also induce *RUNX2* expression after TGF- β 1 and BMP-2 stimulation.⁹³ Taken together, various cytokines and considerable crosstalk among pathways likely contribute to its finely tuned regulation. In fact, by showing that *RUNX2* expression was maintained in OPs without high *FGF1* levels, namely PM- and LP-OPs, our study indicates that *FGF1* is neither an early specifier of the OP lineage nor the sole regulator of *RUNX2*. In the context of osteoblastogenesis, most lines of evidence implicate *FGF2* and *FGF18* as other major players. Disruption of *FGF2* (*FGF2*^{-/-}) in mice causes marked decreases in long bone mass and rate of bone formation, with cultured *FGF2*^{-/-} BMSCs displaying decreased osteoblast differentiation.^{94,95} *FGF18* knockout mice exhibited normal *RUNX2* expression in the perichondrium/periosteum of the humerus, indicating normal OP cell numbers; however, delayed ossification was observed in the cortical bone, which arises from the perichondrium, suggesting *FGF18*'s role in osteoblast maturation and less so in determining OP lineage.⁹⁶ By demonstrating the reduction in *RUNX2* by inhibiting *FGF1*, our study adds to the body of evidence that *FGF1*, like *FGF2*, 4 and 18, is a positive regulator of *RUNX2* but a unique molecule in neural crest-derived osteoblast differentiation.

Lastly, regulation of *RUNX2* also occurs by phosphorylation of specific serine residues. Ser-to-Ala mutations at sites Ser-301 and -319 can diminish its transcriptional activity at promoter regions of other osteogenic genes⁷¹ and interaction with other transcription factors, such as OSTERIX.⁷² Phosphorylation of *RUNX2* appears to mainly involve the MAPK pathway. Transfection of preosteoblast cells with constitutively active MEK1 (MAPK kinase or MAPKK), an upstream activator of ERK1/2, corresponded with an increase in phosphorylation and activity of *RUNX2*,⁷¹ which another study demonstrated occurred by enhancing DNA-binding capacity in the context of *FGF2*.⁹⁷ The decrease in ERK1/2 after *FGF1* inhibition suggested that in addition to influencing expression levels of *RUNX2*, *FGF1* may also regulate its transcriptional activity through MAPK signaling. Although there are still many questions remaining about how *FGF1* influences *RUNX2*, we put forward evidence that *FGF1* is an important molecule in the context of bone formation in NC-OPs. To better describe *FGF1*'s role in the context of craniofacial bone morphogenesis, it will be necessary to further investigate *FGF1*'s receptor binding profile, signaling cascades, and *FGF1*-*RUNX2* pathways in vivo.

The strengths of our study include a comprehensive, reliable list of markers against which the success of the differentiation system was measured; derivation of all three OP lineages in multiple cell lines; in vivo confirmation of OP bone-forming potential; selection of a high threshold for highly expressed genes; and demonstration of *FGF1* expression in vivo and quantification at the protein level. Reflecting lineage-specific developmental processes, our stepwise differentiation system offers a platform to model human bone organogenesis and disease through hPSCs harboring mutations of interest. Additionally, the discovery of *FGF1* in NC-OPs presents an opportunity to explore

its role in neural crest-derived structures, including its receptor binding profile and signaling pathways. Limitations include differences in expression levels and differentiation efficiencies between hiPSCs and hESCs. However, it is not uncommon for cell types to contribute to variation in performance, even when cultured under identical conditions.⁹⁸ For example, in a study generating osteoclasts from hESC- and hiPSC-derived hematopoietic progenitors, the percentage of CD45⁺ cells varied widely across two hESC and one hiPSC lines tested.⁸ These differences may be due, in part, to epigenetic memory or accumulated aberrations during the reprogramming process.⁹⁹ Importantly, however, despite these differences, we emphasize the identity and purity of final differentiated cell populations. Furthermore, although our study provides strong evidence of FGF1's influence on RUNX2, direct confirmation of its role in bone formation will be needed through in vivo studies.

5 | CONCLUSION

An optimized method of differentiating hPSCs into lineage-specific osteogenic populations was developed and validated through extensive characterization at every stage. Differential transcriptomic signatures and shared genes were also identified among OPs, which demonstrated osteogenic potential in vivo, the gold standard by which to determine osteogenic differentiation. The new discovery of high FGF1 found in NC-OPs and its influence on RUNX2 indicates its potentially important role in the development of craniofacial structures. Overall, this study strengthens the utility of hPSCs to model early bone developmental processes.

ACKNOWLEDGMENTS

This work is supported by NIH/NIDCR funding sources: Robey–ZIA DE000380, Lee–ZIA DE000727 and DE022556 (D.S.K.). This research was also made possible, in part, through the NIH Medical Research Scholars Program, a public-private partnership supported jointly by the NIH and contributions to the Foundation for the NIH from the Doris Duke Charitable Foundation, Genentech, the American Association for Dental Research, the Colgate-Palmolive Company, and other private donors. The authors also wish to acknowledge the Fulbright-Nehru Postdoctoral Research Fellowship to D.A. and the NIDCR Combined Technical Research Core, and the NIDCR-NIDCD Genomics and Computational Biology Core for their contributions to this work.

CONFLICT OF INTEREST

D.S.K. declared intellectual property rights with UC-San Diego; advisory role, research finding and ownership interest with Fate Therapeutics. The other authors declared no potential conflicts of interest.

AUTHOR CONTRIBUTIONS

F.K.: conception and design, data analysis and interpretation, manuscript writing, collection and/or assembly of data, final approval of the manuscript; B.M.: collection and/or assembly of data, data analysis and interpretation, manuscript writing; D.A.: collection and/or

assembly of data, data analysis and interpretation; K.I.: assembly of data, data analysis and interpretation, manuscript writing; M. Z., L.F.D.C.D., N.C., D.M., V.D.M., M.A., K.F., R.M.: collection and/or assembly of data; S.A.: manuscript proofread; D.S.K., J.L.: data analysis and interpretation; P.G.R.: conception and design, data analysis and interpretation, manuscript writing, final approval of the manuscript.

DATA AVAILABILITY STATEMENT

The data that support the findings of this study are available from the corresponding author upon reasonable request.

ORCID

Fahad Kidwai  <https://orcid.org/0000-0001-9845-8404>

Dan S. Kaufman  <https://orcid.org/0000-0002-2003-2494>

REFERENCES

- Kanke K, Masaki H, Saito T, et al. Stepwise differentiation of pluripotent stem cells into osteoblasts using four small molecules under serum-free and feeder-free conditions. *Stem Cell Rep.* 2014;2(6):751-760.
- Kornak U, Mundlos S. Genetic disorders of the skeleton: a developmental approach. *Am J Hum Genet.* 2003;73(3):447-474.
- McBratney-Owen B, Iseki S, Olsen BR, et al. Developmental and tissue origins of the mammalian cranial base. *Dev Biol.* 2008; 322(1): 121-132.
- Mahmood A, Napoli C, Aldahmash A. In vitro differentiation and maturation of human embryonic stem cell into multipotent cells. *Stem Cells Int.* 2011;2011:735420.
- Tremoleda JL, Forsyth NR, Khan NS, et al. Bone tissue formation from human embryonic stem cells in vivo. *Cloning Stem Cells.* 2008;10(1): 119-132.
- Zou L, Kidwai FK, Kopher RA, et al. Use of RUNX2 expression to identify osteogenic progenitor cells derived from human embryonic stem cells. *Stem Cell Reports.* 2015;4(2):190-198.
- Phillips MD, Kuznetsov SA, Cherman N, et al. Directed differentiation of human induced pluripotent stem cells toward bone and cartilage: in vitro versus in vivo assays. *STEM CELLS TRANSLATIONAL MEDICINE.* 2014;3 (7):867-878.
- Grigoriadis AE, Kennedy M, Bozec A, et al. Directed differentiation of hematopoietic precursors and functional osteoclasts from human ES and iPS cells. *Blood.* 2010;115(14):2769-2776.
- Tran NT, Trinh QM, Lee GM, et al. Efficient differentiation of human pluripotent stem cells into mesenchymal stem cells by modulating intracellular signaling pathways in a feeder/serum-free system. *Stem Cells Dev.* 2012;21(7):1165-1175.
- Kidwai F, Edwards J, Zou L, et al. Fibrinogen induces RUNX2 activity and osteogenic development from human pluripotent stem cells. *STEM CELLS.* 2016;34(8):2079-2089.
- Fantl WJ, Johnson DE, Williams LT. Signalling by receptor tyrosine kinases. *Annu Rev Biochem.* 1993;62:453-481.
- Ornitz DM, Marie PJ. Fibroblast growth factor signaling in skeletal development and disease. *Genes Dev.* 2015;29(14):1463-1486.
- Su N, Jin M, Chen L. Role of FGF/FGFR signaling in skeletal development and homeostasis: learning from mouse models. *Bone Res.* 2014; 2:14003.
- Goetz R, Mohammadi M. Exploring mechanisms of FGF signalling through the lens of structural biology. *Nat Rev Mol Cell Biol.* 2013;14 (3):166-180.
- Turner N, Grose R. Fibroblast growth factor signalling: from development to cancer. *Nat Rev Cancer.* 2010;10(2):116-129.
- Komori T. Regulation of osteoblast differentiation by transcription factors. *J Cell Biochem.* 2006;99(5):1233-1239.

17. Tan JY, Sriram G, Rufaihah AJ, Neoh KG, Cao T. Efficient derivation of lateral plate and paraxial mesoderm subtypes from human embryonic stem cells through GSKi-mediated differentiation. *Stem Cells Dev.* 2013; 22(13):1893–1906. <https://doi.org/10.1089/scd.2012.0590>.
18. Fukuta M, Nakai Y, Kirino K, et al. Derivation of mesenchymal stromal cells from pluripotent stem cells through a neural crest lineage using small molecule compounds with defined media. *PLoS One.* 2014;9(12):e112291.
19. Donaldson JG. Immunofluorescence staining. *Curr Protoc Cell Biol.* 1998; Chapter 4:Unit 4.3.00 4.3.1–4.3.6.
20. Myneni VD, Hitomi K, Kaartinen MT. Factor XIII-A transglutaminase acts as a switch between preadipocyte proliferation and differentiation. *Blood.* 2014;124(8):1344–1353.
21. Dobin AY, Victora RH. Intrinsic nonlinear ferromagnetic relaxation in thin metallic films. *Phys Rev Lett.* 2003;90(16):167203.
22. Hartley SW, Mullikin JC. QoRTs: a comprehensive toolset for quality control and data processing of RNA-Seq experiments. *BMC Bioinformatics.* 2015;16:224.
23. Love MI, Huber W, Anders S. Moderated estimation of fold change and dispersion for RNA-seq data with DESeq2. *Genome Biol.* 2014;15(12):550.
24. Robinson MD, McCarthy DJ, Smyth GK. edgeR: a Bioconductor package for differential expression analysis of digital gene expression data. *Bioinformatics.* 2010;26(1):139–140.
25. Law CW, Chen Y, Shi W, et al. voom: precision weights unlock linear model analysis tools for RNA-seq read counts. *Genome Biol.* 2014;15(2):R29.
26. Gadue P, Huber TL, Paddison PJ, et al. Wnt and TGF-beta signaling are required for the induction of an in vitro model of primitive streak formation using embryonic stem cells. *Proc Natl Acad Sci U S A.* 2006; 103(45):16806–16811.
27. Sumi T, Tsuneyoshi N, Nakatsuji N, et al. Defining early lineage specification of human embryonic stem cells by the orchestrated balance of canonical Wnt/beta-catenin, Activin/Nodal and BMP signaling. *Development.* 2008;135(17):2969–2979.
28. Faial T, Bernardo AS, Mendjan S, et al. Brachyury and SMAD signaling collaboratively orchestrate distinct mesoderm and endoderm gene regulatory networks in differentiating human embryonic stem cells. *Development.* 2015;142(12):2121–2135.
29. Rosa A, Papaioannou MD, Krzyspiak JE, et al. miR-373 is regulated by TGFbeta signaling and promotes mesendoderm differentiation in human embryonic stem cells. *Dev Biol.* 2014;391(1):81–88.
30. Saga Y, Hata N, Kobayashi S, et al. MesP1: a novel basic helix-loop-helix protein expressed in the nascent mesodermal cells during mouse gastrulation. *Development.* 1996;122(9):2769–2778.
31. Peterson RS, Lim L, Ye H, et al. The winged helix transcriptional activator HFH-8 is expressed in the mesoderm of the primitive streak stage of mouse embryos and its cellular derivatives. *Mech Dev.* 1997; 69(1–2):53–69.
32. Loh KM, Chen A, Koh PW, et al. Mapping the pairwise choices leading from pluripotency to human bone, heart, and other mesoderm cell types. *Cell.* 2016;166(2):451–467.
33. Sakurai H, Era T, Jakt LM, et al. In vitro modeling of paraxial and lateral mesoderm differentiation reveals early reversibility. *STEM CELLS.* 2006;24(3):575–586.
34. Kataoka H, Takakura N, Nishikawa S, et al. Expressions of PDGF receptor alpha, c-Kit and Flk1 genes clustering in mouse chromosome 5 define distinct subsets of nascent mesodermal cells. *Dev Growth Differ.* 1997;39(6):729–740.
35. Umeda K, Zhao J, Simmons P, et al. Human chondrogenic paraxial mesoderm, directed specification and prospective isolation from pluripotent stem cells. *Sci Rep.* 2012;2:455.
36. Chapman DL, Agulnik I, Hancock S, et al. Tbx6, a mouse T-Box gene implicated in paraxial mesoderm formation at gastrulation. *Dev Biol.* 1996;180(2):534–542.
37. Bartscher I, Lickert H. Foxa2 regulates polarity and epithelialization in the endoderm germ layer of the mouse embryo. *Development.* 2009; 136(6):1029–1038.
38. Pesce M, Scholer HR. Oct-4: gatekeeper in the beginnings of mammalian development. *STEM CELLS.* 2001;19(4):271–278.
39. Shalaby F, Ho J, Stanford WL, et al. A requirement for Flk1 in primitive and definitive hematopoiesis and vasculogenesis. *Cell.* 1997;89 (6):981–990.
40. Ema M, Takahashi S, Rossant J. Deletion of the selection cassette, but not cis-acting elements, in targeted Flk1-lacZ allele reveals Flk1 expression in multipotent mesodermal progenitors. *Blood.* 2006;107(1):111–117.
41. Evseenko D, Zhu Y, Schenke-Layland K, et al. Mapping the first stages of mesoderm commitment during differentiation of human embryonic stem cells. *Proc Natl Acad Sci.* 2010;107:13742–13747.
42. Flores-Torales E, Orozco-Barocio A, Gonzalez-Ramella OR, et al. The CD271 expression could be alone for establisher phenotypic marker in Bone Marrow derived mesenchymal stem cells. *Folia Histochem Cytobiol.* 2010;48(4):682–686.
43. Alvarez-Viejo M, Menendez-Menendez Y, Otero-Hernandez J. CD271 as a marker to identify mesenchymal stem cells from diverse sources before culture. *World J Stem Cells.* 2015;7(2):470–476.
44. Chawengsaksophak K, de Graaff W, Rossant J, et al. Cdx2 is essential for axial elongation in mouse development. *Proc Natl Acad Sci U S A.* 2004;101(20):7641–7645.
45. Chalamalasetty RB, Garriock RJ, Dunty WC Jr, et al. Mesogenin 1 is a master regulator of paraxial presomitic mesoderm differentiation. *Development.* 2014;141(22):4285–4297.
46. Outten JT, Cheng X, Gadue P, et al. A high-throughput multiplexed screening assay for optimizing serum-free differentiation protocols of human embryonic stem cells. *Stem Cell Res.* 2011;6(2):129–142.
47. Arnold SJ, Hofmann UK, Bikoff EK, et al. Pivotal roles for eomesodermin during axis formation, epithelium-to-mesenchyme transition and endoderm specification in the mouse. *Development.* 2008;135(3):501–511.
48. Liu Y, Harmelink C, Peng Y, et al. CHD7 interacts with BMP R-SMADs to epigenetically regulate cardiogenesis in mice. *Hum Mol Genet.* 2014;23(8):2145–2156.
49. Riaz AM, Takeuchi JK, Hornberger LK, et al. NKX2-5 regulates the expression of beta-catenin and GATA4 in ventricular myocytes. *PLoS One.* 2009;4(5):e5698.
50. Lin L, Bu L, Cai CL, et al. Isl1 is upstream of sonic hedgehog in a pathway required for cardiac morphogenesis. *Dev Biol.* 2006;295(2):756–763.
51. Chijimatsu R, Ikeya M, Yasui Y, et al. Characterization of mesenchymal stem cell-like cells derived from human iPSCs via neural crest development and their application for osteochondral repair. *Stem Cells Int.* 2017;2017:1960965.
52. Brunskill EW, Potter AS, Distasio A, et al. A gene expression atlas of early craniofacial development. *Dev Biol.* 2014;391(2):133–146.
53. Southard-Smith EM, Kos L, Pavan WJ. Sox10 mutation disrupts neural crest development in Dom Hirschsprung mouse model. *Nat Genet.* 1998;18(1):60–64.
54. Rivera-Pérez JA, Mallo M, Gendron-Maguire M, et al. Gooseoid is not an essential component of the mouse gastrula organizer but is required for craniofacial and rib development. *Development.* 1995;121(9):3005–3012.
55. Rivera-Pérez JA, Wakamiya M, Behringer RR. Gooseoid acts cell autonomously in mesenchyme-derived tissues during craniofacial development. *Development.* 1999;126(17):3811–3821.
56. Yamada G, Mansouri A, Torres M, et al. Targeted mutation of the murine gooseoid gene results in craniofacial defects and neonatal death. *Development.* 1995;121(9):2917–2922.
57. Cheung M, Briscoe J. Neural crest development is regulated by the transcription factor Sox9. *Development.* 2003;130(23):5681–5693.
58. Holland ND, Panganiban G, Henyey EL, et al. Sequence and developmental expression of Amphidil, an amphioxus distal-less gene transcribed in the ectoderm, epidermis and nervous system: insights into evolution of craniate forebrain and neural crest. *Development.* 1996;122(9):2911–2920.
59. Wada RK, Pai DS, Huang J, et al. Interferon-gamma and retinoic acid down-regulate N-myc in neuroblastoma through complementary mechanisms of action. *Cancer Lett.* 1997;121(2):181–188.

60. Inman KE, Caiaffa CD, Melton KR, et al. Foxc2 is required for proper cardiac neural crest cell migration, outflow tract septation, and ventricle expansion. *Dev Dyn*. 2018;247(12):1286-1296.
61. Laurie LE, Kokubo H, Nakamura M, et al. The transcription factor Hand1 is involved in Runx2-lhx-regulated endochondral ossification. *PLoS One*. 2016;11(2):e0150263.
62. Acampora D, Merlo GR, Paleari L, et al. Craniofacial, vestibular and bone defects in mice lacking the distal-less-related gene Dlx5. *Development*. 1999;126(17):3795-3809.
63. Gilbert SF. *Developmental Biology*. 6th ed. Sunderland, MA: Sinauer Associates; 2000.
64. Ornitz DM, Itoh N. The fibroblast growth factor signaling pathway. *Wiley Interdiscip Rev Dev Biol*. 2015;4(3):215-266.
65. Chen F, Hristova K. The physical basis of FGFR3 response to fgf1 and fgf2. *Biochemistry*. 2011;50(40):8576-8582.
66. Thorns V, Licastro F, Masliah E. Locally reduced levels of acidic FGF lead to decreased expression of 28-kda calbindin and contribute to the selective vulnerability of the neurons in the entorhinal cortex in Alzheimer's disease. *Neuropathology*. 2001;21(3):203-211.
67. Tooyama I, Kremer HP, Hayden MR, et al. Acidic and basic fibroblast growth factor-like immunoreactivity in the striatum and midbrain in Huntington's disease. *Brain Res*. 1993;610(1):1-7.
68. Kim HJ, Kim JH, Bae SC, et al. The protein kinase C pathway plays a central role in the fibroblast growth factor-stimulated expression and transactivation activity of Runx2. *J Biol Chem*. 2003;278(1):319-326.
69. Komori T. Molecular mechanism of Runx2-dependent bone development. *Mol Cells*. 2020;43(2):168-175.
70. Zhang X, Schwarz EM, Young DA, Puzas JE, Rosier RN, O'Keefe RJ. Cyclooxygenase-2 regulates mesenchymal cell differentiation into the osteoblast lineage and is critically involved in bone repair. *J Clin Invest*. 2002;109:1405-1415.
71. Xiao G, Jiang D, Gopalakrishnan R, et al. Fibroblast growth factor 2 induction of the osteocalcin gene requires MAPK activity and phosphorylation of the osteoblast transcription factor, Cbfa1/Runx2. *J Biol Chem*. 2002;277(39):36181-36187.
72. Artigas N, Ureña C, Rodríguez-Carballo E, et al. Mitogen-activated protein kinase (MAPK)-regulated interactions between Osterix and Runx2 are critical for the transcriptional osteogenic program. *J Biol Chem*. 2014;289(39):27105-27117.
73. Tonegawa A, Funayama N, Ueno N, et al. Mesodermal subdivision along the mediolateral axis in chicken controlled by different concentrations of BMP-4. *Development*. 1997;124(10):1975-1984.
74. Sancisi V, Gandolfi G, Ragazzi M, et al. Cadherin 6 is a new RUNX2 target in TGF- β signalling pathway. *PLoS One*. 2013;8(9):e75489.
75. Gilchrist A, Stern PH. Editorial: chemokines and bone. *Front Endocrinol (Lausanne)*. 2018;9:386.
76. Conover CA, Lee PD, Riggs BL, et al. Insulin-like growth factor-binding protein-1 expression in cultured human bone cells: regulation by insulin and glucocorticoid. *Endocrinology*. 1996;137(8):3295-3301.
77. Rux DR, Wellik DM. Hox genes in the adult skeleton: novel functions beyond embryonic development. *Dev Dyn*. 2017;246(4):310-317.
78. González-Martín MC, Mallo M, Ros MA. Long bone development requires a threshold of Hox function. *Dev Biol*. 2014;392(2):454-465.
79. Kuznetsov SA, Cherman N, Robey PG. In vivo bone formation by progeny of human embryonic stem cells. *Stem Cells Dev*. 2011;20(2):269-287.
80. Canu N, Pagano I, La Rosa LR, et al. Association of TrkA and APP is promoted by NGF and reduced by cell death-promoting agents. *Front Mol Neurosci*. 2017;10:15.
81. Levi B. "TrkA"cking why "no pain, no gain" is the rule for bone formation. *Sci Transl Med*. 2017;9:eaan3780.
82. Kikuchi K, Fukuda M, Ito T, et al. Transcripts of unknown function in multiple-signaling pathways involved in human stem cell differentiation. *Nucleic Acids Res*. 2009;37(15):4987-5000.
83. Katayama S, Tomaru Y, Kasukawa T, et al. Antisense transcription in the mammalian transcriptome. *Science*. 2005;309(5740):1564-1566.
84. Su N, Du X, Chen L. FGF signaling: its role in bone development and human skeleton diseases. *Front Biosci*. 2008;13:2842-2865.
85. Finch PW, Cunha GR, Rubin JS, et al. Pattern of keratinocyte growth factor and keratinocyte growth factor receptor expression during mouse fetal development suggests a role in mediating morphogenetic mesenchymal-epithelial interactions. *Dev Dyn*. 1995;203(2):223-240.
86. Grottkau BE, Lin Y. Osteogenesis of adipose-derived stem cells. *Bone Res*. 2013;1(2):133-145.
87. Colnot C, Lu C, Hu D, et al. Distinguishing the contributions of the perichondrium, cartilage, and vascular endothelium to skeletal development. *Dev Biol*. 2004;269(1):55-69.
88. Raju R, Palapetta SM, Sandhya VK, et al. A network map of FGF-1/FGFR signaling system. *J Signal Transduct*. 2014;2014:962962.
89. Sasaki T, Ito Y, Bringas P Jr, et al. TGFbeta-mediated FGF signaling is crucial for regulating cranial neural crest cell proliferation during frontal bone development. *Development*. 2006;133(2):371-381.
90. Komori T, Yagi H, Nomura S, et al. Targeted disruption of Cbfa1 results in a complete lack of bone formation owing to maturational arrest of osteoblasts. *Cell*. 1997;89(5):755-764.
91. Enomoto H, Enomoto-Iwamoto M, Iwamoto M, et al. Cbfa1 is a positive regulatory factor in chondrocyte maturation. *J Biol Chem*. 2000;275(12):8695-8702.
92. Niger C, Luciotti MA, Buo AM, et al. The regulation of runt-related transcription factor 2 by fibroblast growth factor-2 and connexin43 requires the inositol polyphosphate/protein kinase C δ cascade. *J Bone Miner Res*. 2013;28(6):1468-1477.
93. Lee KS, Hong SH, Bae SC. Both the Smad and p38 MAPK pathways play a crucial role in Runx2 expression following induction by transforming growth factor-beta and bone morphogenetic protein. *Oncogene*. 2002;21(47):7156-7163.
94. Montero A, Okada Y, Tomita M, et al. Disruption of the fibroblast growth factor-2 gene results in decreased bone mass and bone formation. *J Clin Invest*. 2000;105(8):1085-1093.
95. Xiao L, Sobue T, Eslinger A, et al. Disruption of the Fgf2 gene activates the adipogenic and suppresses the osteogenic program in mesenchymal marrow stromal stem cells. *Bone*. 2010;47(2):360-370.
96. Liu Z, Xu J, Colvin JS, et al. Coordination of chondrogenesis and osteogenesis by fibroblast growth factor 18. *Genes Dev*. 2002;16(7):859-869.
97. Nakahara T, Sato H, Shimizu T, et al. Fibroblast growth factor-2 induces osteogenic differentiation through a Runx2 activation in vascular smooth muscle cells. *Biochem Biophys Res Commun*. 2010;394(2):243-248.
98. Bilic J, Izpissua Belmonte JC. Concise review: induced pluripotent stem cells versus embryonic stem cells: close enough or yet too far apart? *STEM CELLS*. 2012;30(1):33-41.
99. Vaskova EA, Stekleneva AE, Medvedev SP, Zakian SM. "Epigenetic memory" phenomenon in induced pluripotent stem cells. *Acta Nat*. 2013;5(4):15-21.

SUPPORTING INFORMATION

Additional supporting information may be found online in the Supporting Information section at the end of this article.

How to cite this article: Kidwai F, Mui BWH, Arora D, et al. Lineage-specific differentiation of osteogenic progenitors from pluripotent stem cells reveals the FGF1-RUNX2 association in neural crest-derived osteoprogenitors. *Stem Cells*. 2020;38:1107-1123. <https://doi.org/10.1002/stem.3206>